Centroidal Momentum Shaping for Task-Invariant Assistance: Preliminary Validation on a Bilateral Hip Exoskeleton

Miao Yu, Nikhila Krishnan, Jesse Dean, and Ge Lv

Abstract— **Existing control paradigms for lower-limb exoskeletons aim at replicating task-specific, subject-dependent reference kinematics, which overly constrain voluntary human motion. Individuals with voluntary control over their lower-extremities would likely benefit from the ability to choose their gait patterns freely while being assisted by exoskeletons during different activities. In this paper, we propose a novel control paradigm and its implementation to alter a human's Centroidal Momentum, i.e., a sum of projected limb momenta onto the human's center of mass, through tracking a dynamic reference Centroidal Momentum to provide consistent assistance across tasks. This reference Centroidal Momentum is defined based on the human's self-selected gaits with scaled anatomical parameters, rather than reference kinematics of specific locomotor tasks. The resulting control strategy does not prescribe any reference trajectories, providing flexibility for human users. We demonstrate simulation results on a human-like biped and experimental results on four human subjects wearing a bilateral hip exoskeleton performing various walking tasks under different speed and incline/decline conditions. These results show that the generated assistance/resistance can reduce/increase the subjects' muscle efforts, respectively, across the performed tasks.**

I. INTRODUCTION

Emerging powered lower-limb exoskeletons have demonstrated great potential in assisting their human users for various activities [1]. Depending on the intended control and design goals, they can help bear the weight of extra loads [2], reduce energy expenditure [3] during walking, and restore normative gait kinematics [4]. The vast majority of existing control paradigms are trajectory-based that replicate reference kinematics for human user's joints [5], which are appropriate for individuals that with neurological injuries that prevent voluntarily generation of lower extremity motions [5]. For individuals with partial or full voluntary control over their lower extremities (e.g., able-bodied persons), control paradigms would ideally enable exoskeletons to provide assistance without confining their preferred gaits for facilitating the adaptability to various walking patterns [1].

Trajectory-free control approaches do not confine user's joint kinematics to specific gait patterns, and therefore are promising to promote flexibility for humans in choosing their self-preferred gaits [1]. For instance, human muscle activations can be measured via Electromyography (EMG) sensors and used as feedback for exoskeleton control design to assist human locomotion [6], [7]. However, performance of EMG sensors is susceptible and sensitive to measurement noises, placement of electrodes, and sweating [8]. Energy shaping and passivity-based control methods [9]–[11] enable exoskeletons to provide task-invariant assistance through dynamically altering human body energetics. While independent of reference trajectories, solving achievable dynamics for high-dimensional, underactuated systems requires solution to the matching condition [10], which can be very challenging to obtain, especially with varying degrees of underactuation during human locomotion. Although other trajectory-independent control paradigms exist, they are specifically proposed for dedicated tasks such as sit-to-stand [12], stair ascent [13], or walking tasks [3]. It remains unclear if these control paradigms can still demonstrate the same efficacy when translating into continuously varying daily activities.

As a commonly used physical metric in locomotion [14], Centroidal Momentum (CM), the sum of projected segmental momenta onto a robot's Center of Mass (CoM) [15], has been applied in the development of control strategies for both bipeds and quadrupeds [14], [16]. CM has also been used as an index to evaluate the stability of human gaits [17], performance of balance recovery strategies [18], and models that predict human CoM trajectory during sit-to-stand motion [19]. CM is consistently represented as a six-dimensional vector in 3D space [15] regardless of biped models or walking gaits [15], which can be advantageous in designing control strategies to modify it. As long as the number of exoskeleton actuators exceeds six, we can guarantee the existence of a control law to alter a human's CM, even for underactuated systems. Control allocation (i.e., achieving a desired CM with specific actuators) can also be realized, which is usually feasible when the system is overactuated [20]. Finally, altering a human's CM via exoskeleton actuators does not prescribe joint-level kinematics nor specific limb momentum, which has the potential to generate task-invariant assistance and promote voluntary human motion.

In this paper, we propose a control paradigm called CM shaping to alter a human's CM for providing task-invariant assistance, as well as its implementation on a powered bilateral hip exoskeleton. The control law is yielded through tracking the desired CM of a virtual reference model, whose joint kinematics are based on the human user's self-selected gaits and scaled version of limb inertial parameters. Through tracking this reference CM via exoskeleton actuators, we can mimic behaviors of the virtual reference model with altered inertial parameters (greater or less) of a human user (Fig. 1).

This work was supported by the National Science Foundation under Award 2340261. The content is solely the responsibility of the authors and does not necessarily represent the official views of the NSF.

M. Yu, N. Krishnan, and G. Lv are with the Department of Mechanical Engineering, Clemson University, Clemson, SC 29634, USA. Contact: {myu2, nikhila, glv}@clemson.edu. J. Dean is with the Department of Rehabilitation Sciences, Medical University of South Carolina, Charleston, SC 29425, USA. Contact: deaje@musc.edu. Corresponding author: Ge Lv.

We implemented the proposed control strategy on a powered bilateral hip exoskeleton with highly backdrivable actuators, and integrated inertial measurement units (IMUs) into the overall control system for measuring human limb kinematics. A nonlinear disturbance observer (NDO) was proposed to estimate human joint torques for control derivation. Experimental results on four able-bodied participants wearing the hip exoskeleton during walking tasks at varying speeds and slopes demonstrate that the generated assistance/resistance can reduce/increase muscular efforts.

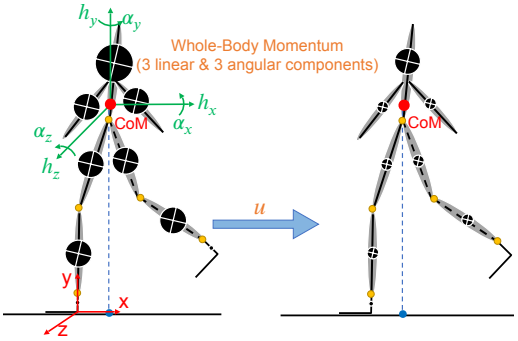

Fig. 1: Concept of CM shaping: through shaping CM of a human via exoskeleton torque u, we can mimic the CM of a lighter person (right) for gait benefits.

II. DYNAMICS & CONTROL METHOD

A. Biped Dynamics

We model a human wearing a lower-limb exoskeleton as a whole biped that ambulates in the sagittal plane, given that the predominant motions during human walking occur in the sagittal plane [21]. Assuming the human-exoskeleton system is a rigid body, its Euler-Lagrange dynamics can be expressed as [22]

$$M\ddot{q}+C\dot{q}+N+A^T\lambda=\tau, \tag{1}$$

where n denotes the number of degrees of freedom (DoFs), $q\in\mathbb{R}^{\mathrm{n}}$ is the configuration vector that will be specified for simulation and experimental models in Sec. IV, $M\in\mathbb{R}^{\mathrm{n}\times\mathrm{n}}$ is the positive-definite inertia matrix, $C\in\mathbb{R}^{\mathrm{n}\times\mathrm{n}}$ is the Coriolis/centrifugal matrix, and $N\in\mathbb{R}^{\mathrm{n}}$ indicates the gravitational force vector. All inertial parameters in these matrices are the sum of the human and exoskeleton inertial parameters. The constraint matrix A, defined as the gradient of holonomic constraint functions, maps the ground reaction force vector $\lambda=\hat{\lambda}+\check{\lambda}\tau$ into the overall dynamics, where $\hat{\lambda}=W(\dot{A}\dot{q}-AM^{-1}N)$, $W=(AM^{-1}A^T)^{-1}$, and $\check{\lambda}=WAM^{-1}$ [22]. The overall torque τ sums up two parts: the human joint torque vector τ_{hum} and the exoskeleton input $\tau_{\mathrm{exo}}=Bu$, where $B=(0_{\mathrm{p}\times\mathrm{n}-\mathrm{p}},\ I_{\mathrm{p}\times\mathrm{p}})^T\in\mathbb{R}^{\mathrm{n}\times\mathrm{p}}$ is the mapping matrix for the exoskeleton torque $u\in\mathbb{R}^{\mathrm{p}}$.

B. Centroidal Momentum Shaping

The CM of a human, $h_G\in\mathbb{R}^{6\times1}$, is defined as the sum of projected limb momenta onto the individual's CoM. Defining $A_G\in\mathbb{R}^{6\times\mathrm{n}}$ as the CM matrix, h_G can be expressed as

$$h_G=A_G\dot{q}. \tag{2}$$

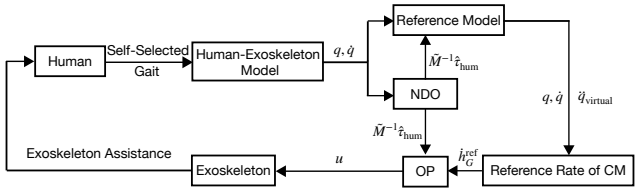

Fig. 2: CM shaping control diagram (reproduced from [23]).

We then propose the following relationship between reference CM h_G^{ref}, h_G, and their derivatives as:

$$\dot{h}_G^{\mathrm{ref}}-\dot{h}_G+K_p(h_G^{\mathrm{ref}}-h_G)=0, \tag{3}$$

where $K_p\in\mathbb{R}^{6\times6}$ is a positive-definite diagonal matrix. We propose this definition to track the change rate of h_G^{ref} meanwhile minimizing the difference between h_G and h_G^{ref}, which is generated only after a human starts walking. Similar to following a target vehicle with varying speeds, we hope to achieve the same velocity for the follower vehicle rather than a desired position over time. Re-writing h_G^{ref} following the convention in (2) and taking its time derivative yields

$$h_G^{\mathrm{ref}}=A_G^{\mathrm{ref}}\dot{q},\quad \dot{h}_G^{\mathrm{ref}}=\dot{A}_G^{\mathrm{ref}}\dot{q}+A_G^{\mathrm{ref}}\ddot{q}, \tag{4}$$

where $\ddot{q}$ can be obtained from a virtual reference model

$$M^{\mathrm{ref}}\ddot{q}+C^{\mathrm{ref}}\dot{q}+N^{\mathrm{ref}}+A^T\lambda^{\mathrm{ref}}=\tau_{\mathrm{hum}}. \tag{5}$$

The matrices M^{ref}, C^{ref}, N^{ref}, and λ^{ref} in (5) are defined similarly to the ones in (1) but with each link's inertial parameters m_i and I_i scaled $k_i\in\mathbb{R}^+$ times, i.e., $m_i^{\mathrm{ref}}=k_im_i$ and $I_i^{\mathrm{ref}}=k_iI_i$. Intuitively, $k_i>1$ (<1) renders resistive (assistive) strategies, as reference CM will be defined with larger (smaller) inertial parameters to reflect a heavier (lighter) person. Equating $\dot{h}_G$ in (3) with $\dot{A}_G\dot{q}+A_G\ddot{q}$, we obtain

$$-A_G\ddot{q}+Y=0, \tag{6}$$

where $Y=-\dot{A}_G\dot{q}+\dot{h}_G^{\mathrm{ref}}+K_p(A_G^{\mathrm{ref}}\dot{q}-A_G\dot{q})$. With the assumption that the human ambulates in the sagittal plane, the CM's linear components along z-axis and angular momenta around x- and y-axes are zeros. Therefore, A_G contains only three non-zero rows, which further simplifies (6) into three equivalent equations. If an exoskeleton has more than three actuators, then there exists infinite solutions to the control law u. We apply an optimization procedure to determine u as

$$\begin{aligned}\min_{u}\quad & u^TWu\\ \text{s.t.}\quad & -A_G\ddot{q}+Y=0,\\ & u_{\min}\le||u||_2\le u_{\max},\end{aligned}$$

where $W\in\mathbb{R}^{\mathrm{p}\times\mathrm{p}}$ is a diagonal, positive-definite weight matrix, $u_{\min},\ u_{\max}\in\mathbb{R}$ are the lower and upper bounds of control torques, respectively. The objective function is chosen as u^TWu to minimize torques exerted by the exoskeleton actuators for energy efficient solutions. Additionally, the weight matrix W can be adjusted to achieve control allocation depending on specific assistive or resistive goals. The above optimization problem can be solved by using the Lagrange multiplier method [24]. Defining the Lagrange multiplier to

be $\eta \in \mathbb{R}^{\mathrm{m}}$, where m is the number of non-zero elements to be shaped in CM, and a Lagrangian $\mathcal{L}(u,\eta) = u^T W u + \eta^T \cdot$ left-hand side of (6), we compute $\partial\mathcal{L}/\partial u = 0$ and plug it into $\partial\mathcal{L}/\partial\eta = 0$ to obtain the CM shaping strategy as

$$u^* = -\frac{1}{2} W^{-1} B_\lambda^T Z^T D^{-1} [Z(C\dot{q} + N + A^T \hat{\lambda} - \tilde{\tau}_{\mathrm{hum}}) + Y], \quad (7)$$

where $B_\lambda = B - A^T \check{\lambda}$, $\tilde{\tau}_{\mathrm{hum}} = (I - A^T \check{\lambda})\tau_{\mathrm{hum}}$, $D = ZB_\lambda W^{-1} B_\lambda^T Z^T$, and $Z = A_G M^{-1}$.

C. Nonlinear Disturbance Observer

The proposed CM shaping strategy (7) requires knowledge of τ_{hum}, which can be difficult to measure in practice. We modify an existing model-based NDO [25] to estimate human joint torques using only angular information. The required sensors for measurements will be discussed in Sec. III-B. Defining $z = M^{-1}\tilde{\tau}_{\mathrm{hum}}$ as the term that needs to be estimated and left-multiplying M^{-1} at both sides of (1), we have

$$z = \ddot{q} + M^{-1} C\dot{q} + M^{-1} N + M^{-1} A^T \hat{\lambda} - M^{-1} B_\lambda u. \quad (8)$$

Denoting $\hat{z}$ as the estimate for z and $e = z - \hat{z}$ as the estimation error, we have [26]:

$$\dot{\hat{z}} = Le = L(z - \hat{z}), \quad (9)$$

where $L \in \mathbb{R}^{\mathrm{n}\times\mathrm{n}}$ can be chosen as a positive-definite, diagonal matrix to guarantee uniformly ultimate boundness and fast convergence of e [26] governed by

$$\dot{e} = \dot{z} - \dot{\hat{z}} = \dot{z} - Le. \quad (10)$$

III. Bilateral Hip Exoskeleton System

To demonstrate efficacy of the proposed method, we implemented the CM shaping strategy (7) on a bilateral, powered hip exoskeleton with highly backdrivable (i.e., low mechanical impedance) actuators and externally integrated sensors (Fig. 3, left). In this section, we introduce the structure of the exoskeleton control system.

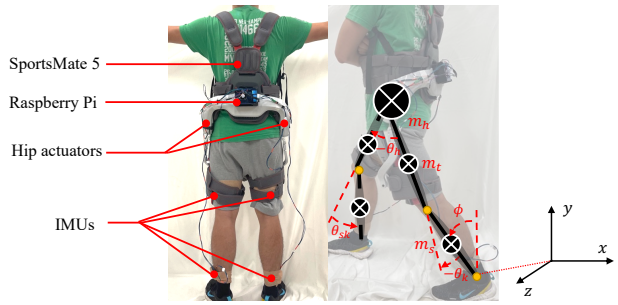

Fig. 3: A participant wearing SportsMate 5 with externally mounted IMUs (left) and configuration variables for the 4-DoF experimental model (right).

A. SportsMate 5 Exoskeleton

SportsMate 5 (Enhanced Power Technology Co., Ltd., Shenzhen, China) has two brushless direct current motors that can produce 7.5 Nm continuous torque (22.5 Nm peak torque) after a 25:1 transmission ratio. The actuators are highly backdrivable (0.096 Nm backdrive torque) to allow voluntary human motion. It also includes two magnetic absolute joint encoders (with embedded Kalman filters) and current sensors to realize closed-loop torque control at 400 Hz on a GD32F303RE microprocessor (ARM Cortex-M4, 120 MHz, 512 kB ROM, 64 kB RAM). The microprocessor is equipped with a UART port and a Bluetooth module to allow for external communication. The exoskeleton weighs about 3.2 kg including a 3200 mAh onboard Lithium battery.

B. Human Kinematics Measurement

To measure human limb kinematics for control calculation, we integrated IMU sensors (NGIMU, x-io Technologies Limited, Bristol, UK) at shanks and thighs (Fig. 3, left) to measure the configuration vector of the human experimental model (will be specified in Sec. IV-B). The IMUs are embedded with an AHRS fusion algorithm [27] to smooth out its output, which is then fitted to a Raspberry Pi 4B (8GB LPDDR4-3200 SDRAM, Quad core Cortex-A72 64-bit SoC, 1.8 GHz) through the UART protocol. Once angular positions are measured, we take numerical derivatives to obtain the corresponding angular velocities and accelerations, where a moving average filter with window size of 71 was applied to attenuate noises in accelerations.

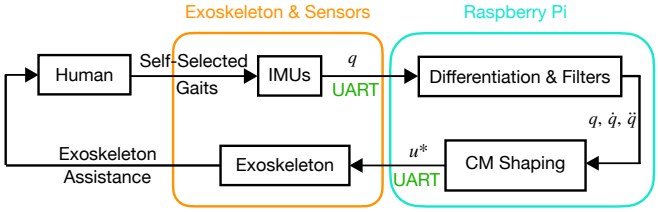

Fig. 4: Overall hardware structure of the exoskeleton system.

C. Control Architecture

The overall control hierarchy in Fig. 4 consists of two layers: a high-level layer that computes u^* in (7) and a low-level layer that achieves the desired torques. Due to limited computation capability of SportsMate 5's microprocessor, we used the Raspberry Pi to communicate with IMUs and compute the torque command in C at about 150 Hz in real time and sent it to SportsMate 5's microprocessor through serial communication. SportsMate 5's embedded motor driver (ER-Driver) will regulate actuator currents to achieve the desired torque through a torque controller with the torque constant of 0.083 Nm/A. Note that the proposed control can be updated on the Raspberry Pi at 550 Hz, but we deliberately reduced the calculation speed to match SportsMate 5's communication frequency.

IV. Simulations & Experiments

In this section, we present simulation results of CM shaping on an 8-DoF dynamic biped and experimental results on four able-bodied human subjects wearing SportsMate 5 during various treadmill walking tasks.

A. Simulation Study

The 8-DoF dynamic biped (Fig. 1, [11]) used in simulation study can walk down a shallow slope with carefully-selected parameters. The biped's configuration vector is given as $q_{\mathrm{sim}} = \{\mathrm{x}, \mathrm{y}, \phi, \theta_{\mathrm{a}}, \theta_{\mathrm{k}}, \theta_{\mathrm{h}}, \theta_{\mathrm{sk}}, \theta_{\mathrm{sa}}\} \in \mathbb{R}^8$, where (x, y) is the position for the inertial reference frame, θ_i, $i \in \{\mathrm{a}, \mathrm{k}, \mathrm{h}, \mathrm{sk}, \mathrm{sa}\}$ indicates the relative angle of stance ankle, stance knee,

hip, swing knee, and swing ankle joints, respectively. Each of these joints is actuated by an exoskeleton actuator, i.e., $u = \{u_a, u_k, u_h, u_{sk}, u_{sa}\} \in \mathbb{R}^5$ and a human joint torque v_i, $i \in \{a, k, h, sk, sa\}$. The overall human torque vector $v \in \mathbb{R}^5$ takes the form $v = -K_p^v(q_{sim} - \bar{q}_{sim}) - K_d^v \dot{q}_{sim}$. Positive-definite matrices K_p^v and K_d^v include proportional and derivative gains, and $\bar{q}_{sim}$ is the equilibrium vector of human joints. We first tuned the gains in K_p^v, K_d^v and $\bar{q}_{sim}$ by trial and error to find a stable passive gait and then implemented u^* for simulations. All simulation parameters can be found in Table II of [11].

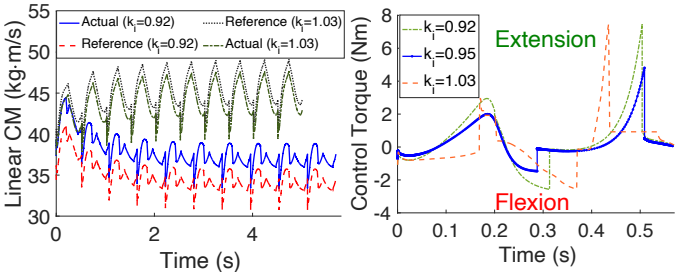

Fig. 5: Simulated linear CM along x-axis (left) and control torque during one steady step (right) with $k_i = 0.92$, 0.95, 1.03, and $K_p = 10 \cdot I_{6\times6}$.

The linear component of CM along the walking direction with k_i = 0.92 (assistive) and 1.03 (resistive) across 8 steps is demonstrated in Fig. 5. We can see that all CM curves preserve similar shapes but with different magnitudes, and the steady errors between the CM of (5) and (1) are caused by the parameter differences between A_G and A_G^{ref} at the beginning of the first step. This difference can lead to continuous tracking action from the exoskeleton, where control torque with k_i = 0.92, 0.95, and 1.03 during one-steady step is shown on the right of Fig. 5. We will compare the simulated control torque with experimental torque results in Sec. IV-D.

B. 4-DoF Experimental Biped Model

SportsMate 5 is equipped with two hip actuators to assist hip flexion/extension during locomotion, which is unlikely to have significant impacts on ankle joints. We therefore adopted a 4-DoF point-feet biped model [28] to derive u^* for experiments considering computational complexity. The configuration vector of this model is given as $q_{exp} = (\phi, \theta_k, \theta_h, \theta_{sk})^T \in \mathbb{R}^4$ (Fig. 3, right) and was measured by four IMU sensors attached at the shank and thigh of both legs. To avoid using additional force sensors on human feet, we set $\hat{\lambda} = 0$ in (7) thus $B_\lambda = B$, $\tilde{\tau}_{hum} = \tau_{hum}$. Inertial terms of humans are estimated following the methods in [29].

The experimental model is defined based on an inertial reference frame (IRF) located at the stance foot. To handle IRF change during stance leg switches, we defined two 4-DoF point-feet biped models: one based at the left foot and the other one at the right. During each leg's stance phase, we applied the corresponding model for that side to compute u^*. The stance leg switches are detected when the hip angular velocity reaches zero, i.e., the onset of the double support phase [30]. In this paper, we chose to shape the linear component of CM along y-axis, as this choice generated the best simulation performance among all non-zero components. We saturated the actuator torques at $\pm$10 Nm to ensure safety, and we assumed each actuator contributed equally to the torque command u^* but in opposite directions throughout the gait cycle as left and right hip torques are roughly symmetric [30], [31].

C. Experimental Protocol

We enrolled 4 able-bodied human subjects (s1: male, 60.4 kg, 1.65 m; s2: female, 60.1 kg, 1.7 m; s3: male, 62.6 kg, 1.76 m; s4: female, 63 kg, 1.62 m) for the experiments. The experimental protocol was approved by the Institutional Review Board of Clemson University (IRB2022-0322), and subject consent was obtained prior to the start of all experiments. All subjects walked on an instrumented treadmill (Bertec Corporation, OH, US) with various speeds and inclines/declines while wearing SportsMate 5.

The experiments for each participant were divided into 8 groups, where each group contained three control modes, i.e., passive ("P", $k_i = 1$, zero actuator torques), resistive ("R", $k_i = 1.2$), and assistive ("A", $k_i = 0.85$), respectively. The speeds and incline conditions for each group are summarized in Table. I, where LG, RA, and RD denote level ground walking, 5° ramp ascent and $-5°$ ramp descent, respectively. For the rest of the paper, we will represent the groups and modes using their acronyms and indices, e.g., A1 indicates the assistive mode in Group 1. Throughout all experiments, we selected $K_p = 10$ and $L = 100 \cdot I_{4\times4}$ for the NDO. The ramp descent scenarios were conducted only with 0.8 m/s and 1 m/s, as the maximum treadmill speed for declined walking is 1 m/s.

During experiments, we first allowed the subject's gaits to converge before data collection. For assistive/resistive trails, subjects were not informed with the underlying control mode. Instead, we asked them to provide feedback on their perceived control modes afterward. All recorded data was cropped into gait cycles by heel strikes detected by two instrumented force plates embedded with the treadmill. We also recorded muscle activations of Rectus Femoris (RF), Biceps Femoris (BF), and Gluteus Maximus (GM) via EMG sensors (Trigno Avanti Sensor, Delsys Inc.), where RF functions as a hip flexor, and BF, GM as hip extensors [32]. The EMG data were first filtered by a fourth-order bandpass filter (20-500 Hz) and rectified, then by a 6 Hz low-pass filter and rectified [33]. The EMG data were then normalized with respect to the maximum peak of the ensemble averages (across repetitions) of three trials within each group. This converted the EMG signals to a percentage of the peak filtered EMG value during the walking trials. After normalizing the EMG to peak EMG (%), we calculated the integral with respect to gait cycle to represent muscular effort.

TABLE I: Experiment Scenarios per Participant

Group	1	2	3	4	5	6	7	8
Speed (m/s)	0.8	1	1.2	0.8	1	1.2	0.8	1
Condition	LG	LG	LG	RA	RA	RA	RD	RD

D. Results & Discussions

For each control mode, we recorded data of 20 steady steps (10 strides) and calculated mean and standard deviation

(SD) of torques, CM, and EMG, where experimental results are shown in Figs. 6 - 10. In all figures, 0% of the gait cycle corresponds to heel strike of the stance leg, and positive/negative torque directions indicate hip flexion/extension, respectively. During experiments, all assistive/resistive trials were successfully recognized by the participants except for 2 trials, and they reported felt less/more required effort when walking with the perceived assistance/resistance, respectively.

The estimated hip torques using NDO (Fig. 6) demonstrate consistent shapes in all control modes. Note that the estimated torques have similar magnitudes but different shapes than those in Winter's data set [30]. This is mainly because the NDO was based on the simplified 4-DoF experimental model from Sec. IV-B that does not fully reflect real human motions. The model also combined two hip joints into one, therefore the estimated torques are the combined torques of both hip joints. Nevertheless, we will see benefits such as reduced muscle activations of the generated assistance/resistance based on the estimated hip torque.

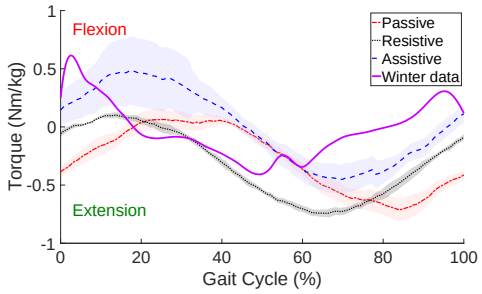

Fig. 6: Mean and $\pm$ 0.5·SD of the estimated hip torques of subject s2 during G2.

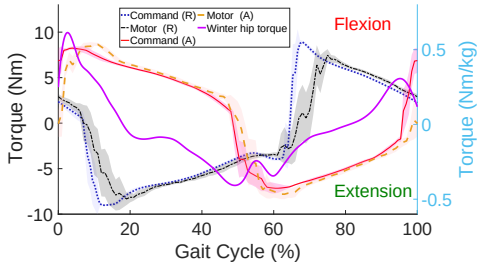

Fig. 7: Mean and $\pm$ 0.5·SD of command and real actuator torques of subject s1 for both A2 and R2 modes.

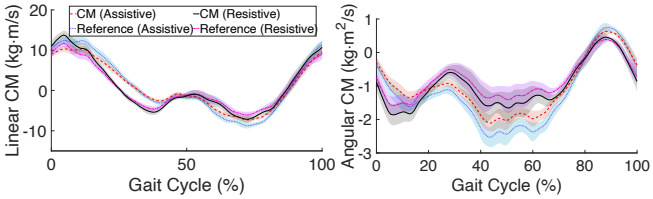

Fig. 8: Mean and $\pm$ 0.5·SD of actual and reference CM (y-axis linear component, left) and (z-axis angular component, right) of s2 during A2 and R2 modes.

The command and tracking torques are shown in Fig. 7. In order to demonstrate the actuators' torque tracking performance, we calculated the command torque offline when the participant walked with the exoskeleton, and then executed the recorded torque command in real-time and recorded the actual generated torque from the actuators. We can see that the actuators can correctly execute command torques. Comparing Fig. 7 with Fig. 5, we can see that experimental torques are very similar to the simulated ones in terms of the torque direction during most part of the gait cycle. In Fig. 8, CM's magnitude, particularly the angular component, is lower in the resistive mode compared to the assistive mode, as the exoskeleton is designed to mimic the behavior of a heavier person. With human inputs from the same participant, this should result in reduced leg segment velocities and consequently a lower CM.

EMG results of sample participants are demonstrated in Fig. 9. Resistive mode in general resulted in higher EMG values thus increased muscle efforts, in terms of either maximum peak (e.g., left RF of s1 in Group 3), or prolonged muscular utilization (e.g., left GM of s1 in Group 3). On the contrary, assistive mode reduced muscle activities, e.g., right BF of s1 in Group 3 and left GM of s2 in Group 4, which coincides with the subjects' qualitative feedback that assistive mode results in less effort especially in the tasks that typically demand more muscle effort than usual, such as ramp ascending (Group 4 in Fig. 9).

Some assistive trials show higher EMG activity in certain muscles compared to passive mode, likely due to two reasons. The participants in this study had no prior experiences with the exoskeleton, their performance could possibly improve over time. The control parameters were consistent across subjects, which may not perfectly align with all subject's preferences. For example, s4's left RF in Group 2 shows a delayed onset compared to other subjects, closely coinciding with the torque transition from flexion to extension that could lead to higher EMG peaks. The control torques in Fig. 7 agree with the above observations. During the first half of a gait cycle, the assistive mode provides flexion torque and this coincides with the onset of RF in Fig. 9 that functions as a hip flexor. Similarly, the extension torque during the second half of the gait cycle coincides with the onset of BF in Fig. 9.

Finally, Fig. 10 shows the integrated EMG (IEMG) ratios between the assistive/resistive modes and the passive mode. Compared to the passive mode, each subject's GM has consistently lower/higher IEMG ratios during most of the assistive/resistive modes. It is evident that almost all muscles have increased effort in all resistive trials. This aligns with the subjects' feedback that during their perceived resistive modes, they felt harder to walk, especially during ramp ascending tasks. In some cases, such as right BF of s1 in A3 (see Fig. 9), the assistive mode results in lower peaks, which could be beneficial, but slightly larger EMG during some parts of the gait cycle result in larger accumulated value.

V. CONCLUSIONS

In this paper, we proposed a task-invariant CM shaping paradigm that assists/resists human locomotion by altering the human's CM. By defining a virtual reference model based on the human user's self-selected gaits and scaled inertial parameters, the proposed shaping strategy tracks the reference

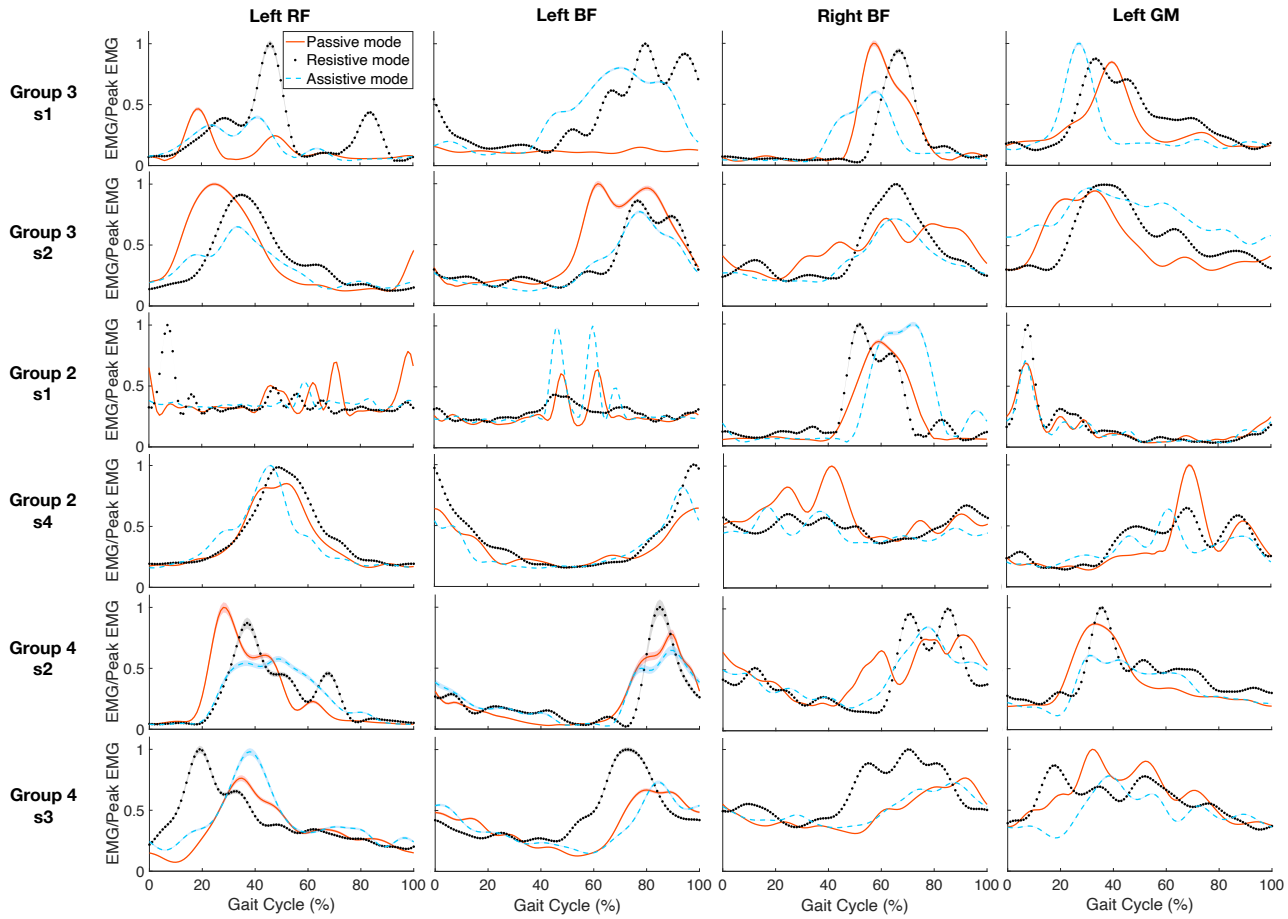

Fig. 9: Mean and ±1·SD EMG results of s1-s4.

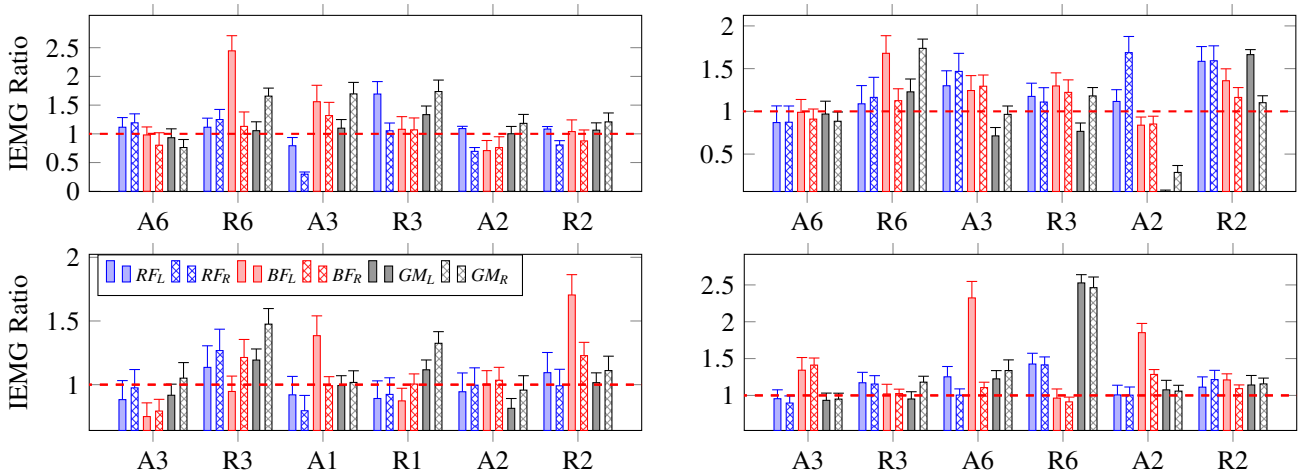

Fig. 10: Mean and 1·SD of IEMG ratio (Controlled/Passive) from s1 (bottom-left) to s4 (bottom-right). For each graph, the first/second/third A-R pair shows the best/worst/average results among 8 groups.

CM to dynamically mimic the gaits of a lighter/heavier person. Simulation studies on an 8-DoF dynamic biped demonstrated that our proposed method successfully altered the biped's CM with reasonable torques. Experimental results on four able-bodied subjects performing different walking tasks demonstrated reduction/increments in muscle activations with assistance/resistance. These results provide a promising foundation for extending this control paradigm to individuals with a reduced ability to voluntarily produce efficient, safe lower extremity motions while walking. The type of assistance delivered here has the potential to allow such individuals to achieve a wider range of gait patterns, with the potential long-term effect on improving functional mobility. Future work includes investigating shaping other CM components and incorporating learning techniques to dynamically customize shaping parameters (K_p, k_i) based on user preferences.

REFERENCES

[1] R. Baud, A. R. Manzoori, A. Ijspeert, and M. Bouri, "Review of control strategies for lower-limb exoskeletons to assist gait," *J. NeuroEng. Rehabil.*, vol. 18, no. 1, pp. 1–34, 2021.

[2] T. Wang, Y. Zhu, T. Zheng, D. Sui, S. Zhao, and J. Zhao, "Palexo: A parallel actuated lower limb exoskeleton for high-load carrying," *IEEE Access*, vol. 8, pp. 67 250–67 262, 2020.

[3] Q. Zhang, V. Nalam, X. Tu, M. Li, J. Si, M. D. Lewek, and H. H. Huang, "Imposing healthy hip motion pattern and range by exoskeleton control for individualized assistance," *IEEE Robot. Autom. Lett.*, vol. 7, no. 4, pp. 11 126–11 133, 2022.

[4] B. Johnson and M. Goldfarb, "A preliminary study on the feasibility of using a knee exoskeleton to reduce crouch gait in an adult with cerebral palsy," in *Int. Conf. Biomed. Robot. Biomechatronics*. IEEE, 2020, pp. 48–53.

[5] T. Yan, M. Cempini, C. M. Oddo, and N. Vitiello, "Review of assistive strategies in powered lower-limb orthoses and exoskeletons," *Robot. Auton. Syst.*, vol. 64, pp. 120–136, 2015.

[6] H. Hsu, I. Kang, and A. J. Young, "Design and evaluation of a proportional myoelectric controller for hip exoskeletons during walking," in *Dyn. Syst. Control Conf.*, vol. 51890. ASME, 2018, p. V001T13A005.

[7] S. Y. Gordleeva, S. A. Lobov, N. A. Grigorev, A. O. Savosenkov, M. O. Shamshin, M. V. Lukoyanov, M. A. Khoruzhko, and V. B. Kazantsev, "Real-time EEG–EMG human–machine interface-based control system for a lower-limb exoskeleton," *IEEE Access*, vol. 8, pp. 84 070–84 081, 2020.

[8] A. J. Young and D. P. Ferris, "State of the art and future directions for lower limb robotic exoskeletons," *IEEE Trans. Neural Syst. Rehabil. Eng.*, vol. 25, no. 2, pp. 171–182, 2016.

[9] J. Lin, N. V. Divekar, G. Lv, and R. D. Gregg, "Optimal task-invariant energetic control for a knee-ankle exoskeleton," *Control Syst. Lett.*, vol. 5, no. 5, pp. 1711–1716, 2020.

[10] G. Lv, H. Zhu, and R. D. Gregg, "On the design and control of highly backdrivable lower-limb exoskeletons: A discussion of past and ongoing work," *IEEE Control Syst. Mag.*, vol. 38, no. 6, pp. 88–113, 2018.

[11] G. Lv, J. Lin, and R. D. Gregg, "Trajectory-free control of lower-limb exoskeletons through underactuated total energy shaping," *IEEE Access*, vol. 9, pp. 95 427–95 443, 2021.

[12] M. K. Shepherd and E. J. Rouse, "Design and validation of a torque-controllable knee exoskeleton for sit-to-stand assistance," *IEEE/ASME Trans. Mechatron.*, vol. 22, no. 4, pp. 1695–1704, 2017.

[13] W. Ma, H. Cheng, R. Huang, and Q. Chen, "Gait planning with dynamic movement primitives for lower limb exoskeleton walking upstairs," in *IEEE Int. Conf. Robot. Biomim*, Dec. 2018, pp. 703–708.

[14] T. Koolen, S. Bertrand, G. Thomas, T. De Boer, T. Wu, J. Smith, J. Englsberger, and J. Pratt, "Design of a momentum-based control framework and application to the humanoid robot atlas," *Int. J. Humanoid Robot.*, vol. 13, no. 01, p. 1650007, 2016.

[15] D. E. Orin, A. Goswami, and S.-H. Lee, "Centroidal dynamics of a humanoid robot," *Auton. Robots*, vol. 35, no. 2, pp. 161–176, 2013.

[16] M. Liu, D. Qu, F. Xu, F. Zou, P. Di, and C. Tang, "Quadrupedal robots whole-body motion control based on centroidal momentum dynamics," *Appl. Sci.*, vol. 9, no. 7, p. 1335, 2019.

[17] J. H. Jung, L. V. Opheusden, P. Barralon, and J. F. Veneman, "Real time computation of centroidal momentum for the use as a stability index applicable to human walking with exoskeleton," in *Wearable Robotics: Challenges and Trends*. Springer, 2017, pp. 157–161.

[18] C. Bayon, A. Emmens, M. Afschrift, T. Van Wouwe, A. Keemink, H. Van Der Kooij, and E. Van Asseldonk, "Can momentum-based control predict human balance recovery strategies?" *IEEE Trans. Neural Syst. Rehabil. Eng.*, vol. 28, no. 9, pp. 2015–2024, 2020.

[19] G. Patil, L. Rigoli, M. J. Richardson, M. Kumar, and T. Lorenz, "Momentum-based trajectory planning for lower-limb exoskeletons supporting sit-to-stand transitions," *Int. J. Intell. Robot. Appl.*, vol. 2, no. 2, pp. 180–192, 2018.

[20] A. Casavola and E. Garone, "Fault-tolerant adaptive control allocation schemes for overactuated systems," *Int. J. Robust Nonlinear Control*, vol. 20, no. 17, pp. 1958–1980, 2010.

[21] M. Q. Liu, F. C. Anderson, M. G. Pandy, and S. L. Delp, "Muscles that support the body also modulate forward progression during walking," *J. Biomech.*, vol. 39, no. 14, pp. 2623–2630, 2006.

[22] R. M. Murray, Z. Li, and S. S. Sastry, *A mathematical introduction to robotic manipulation*. NW Boca Raton, FL: CRC press, 2017.

[23] M. Yu and G. Lv, "Task-invariant centroidal momentum shaping for lower-limb exoskeletons," in *Conf. Decis. Control*. IEEE, 2022, pp. 2054–2060.

[24] R. T. Rockafellar, "Lagrange multipliers and optimality," *SIAM review*, vol. 35, no. 2, pp. 183–238, 1993.

[25] W.-H. Chen, D. J. Ballance, P. J. Gawthrop, and J. O'Reilly, "A nonlinear disturbance observer for robotic manipulators," *IEEE Trans. Ind. Electron.*, vol. 47, no. 4, pp. 932–938, 2000.

[26] H. K. Khalil, *Nonlinear systems; 3rd ed.* Upper Saddle River, NJ: Prentice-Hall, 2002.

[27] S. Madgwick *et al.*, "An efficient orientation filter for inertial and inertial/magnetic sensor arrays," *Report x-io and University of Bristol (UK)*, vol. 25, pp. 113–118, 2010.

[28] E. R. Westervelt, J. W. Grizzle, C. Chevallereau, J. H. Choi, and B. Morris, *Feedback control of dynamic bipedal robot locomotion*. NW Boca Raton, FL: CRC press, 2018.

[29] R. M. Enoka, *Neuromechanics of human movement*. Hum. Kinet., 2008.

[30] D. A. Winter, *Biomechanics and motor control of human movement*. John Wiley & Sons, 2009.

[31] J. Lee, M. E. Huber, and N. Hogan, "Gait entrainment to torque pulses from a hip exoskeleton robot," *Trans. Neural Syst. Rehabil. Eng.*, vol. 30, pp. 656–667, 2022.

[32] D. A. Neumann, "Kinesiology of the hip: a focus on muscular actions," *J Orthop Sports Phys Ther.*, vol. 40, no. 2, pp. 82–94, 2010.

[33] T. Parr, "Development of a novel predictive model and prosthetic system to assess dynamic leg length based gait biomechanics in lower limb prosthesis users," Ph.D. dissertation, Clemson University, 2023.